

---

# Comparing Filtered Backprojection and Ordered-Subsets Expectation Maximization for Small-Lesion Detection and Localization in $^{67}\text{Ga}$ SPECT

R. Glenn Wells, Michael A. King, Peter H. Simkin, Philip F. Judy, A. Bertrand Brill, Howard C. Gifford, Robert Licho, P. Hendrik Pretorius, Peter B. Schneider, and David W. Seldin

*University of Massachusetts Medical Center, Worcester; Brigham and Women's Hospital, Boston; and Lahey Clinic Medical Center, Burlington, Massachusetts*

---

Iterative reconstruction of SPECT images has recently become clinically available as an alternative to filtered backprojection (FBP). However, there is conflicting evidence on whether iterative reconstruction, such as with the ordered-subsets expectation maximization (OSEM) algorithm, improves diagnostic performance over FBP. The study objective was to determine if the detection and localization of small lesions in simulated thoracic gallium SPECT images are better with OSEM reconstruction than with FBP, both with and without attenuation correction (AC). **Methods:** Images were simulated using an analytic projector acting on the mathematic cardiac torso computer phantom. Perfect scatter rejection was assumed. Lesion detection accuracy was assessed using localization receiver operating characteristic methodology. The images were read by 5 nuclear medicine physicians. For each reconstruction strategy and for each observer, data were collected in 2 viewing sessions of 100 images. Two-way ANOVA and, when indicated, the Scheffé multiple comparisons test were applied to check for significant differences. **Results:** Little difference in the accuracy of detection or localization was seen between FBP with and without AC. OSEM with AC extended the contrast range for accurate lesion detection and localization over that of the other methods investigated. Without AC, no significant difference between OSEM and FBP reconstruction was detected. **Conclusion:** OSEM with AC may improve the detection and localization of thoracic gallium-labeled lesions over FBP reconstruction.

**Key Words:** localization receiver operating characteristic; filtered backprojection; ordered-subsets expectation maximization; attenuation correction

**J Nucl Med 2000; 41:1391–1399**

---

**I**maging with  $^{67}\text{Ga}$  is important for assessing both Hodgkin's disease and non-Hodgkin's lymphoma. Gallium scans are useful in the staging of disease, in the detection of

residual tumor during follow-up, in predicting the response to therapy, and in prognosis (1,2). They are also an important complement to MRI and CT because they distinguish viable from necrotic tumor cells. However, a problem with gallium scans is their poor spatial resolution, which, for small (<2 cm) lesions, reduces the apparent contrast because of the partial-volume effect. Even more critical for small lesions, therefore, than for large tumors is improvement of image quality, with reduction of distractions and artifacts that cause inaccurate evaluations. Two techniques that may improve image quality have recently become more readily available for clinical practice: iterative reconstruction and transmission-based attenuation correction (AC).

Because of increases in computer power and improvements in reconstruction algorithms, iterative reconstruction has become a clinically practical alternative to filtered backprojection (FBP). Iterative reconstruction techniques, such as maximum-likelihood expectation maximization (MLEM) or the similar but faster ordered-subsets expectation maximization (OSEM), are attractive because they allow more accurate modeling of the imaging system by including such elements as the positivity constraints on the reconstruction and the Poisson distribution of the projection data. Iterative reconstruction has improved noise properties over FBP, such as reducing the noise correlation length at low numbers of iterations. Thus, MLEM produces less bleeding of high-count noise into low-count regions, potentially improving lesion detection (3–7). Detecting lesions in a low-count, variably attenuating background with nearby high-count background structures is precisely the situation one encounters with gallium imaging because of uptake of gallium in the bones, liver, and heart. This situation might also be encountered with other modalities, such as FDG imaging for detection of lung lesions or whole-body PET.

Studies have shown that iterative reconstruction is better than FBP in tumor detection with whole-body PET, as measured by the signal-to-noise ratio (6) or numeric observers (7). Receiver operating characteristic (ROC) experi-

---

Received Jul. 16, 1999; revision accepted Nov. 2, 1999.  
For correspondence or reprints contact: R. Glenn Wells, PhD, Division of Nuclear Medicine, University of Massachusetts Medical Center, Worcester, MA 01655.

ments using human observers have also shown MLEM to be better than FBP in tumor detection with brain PET (8), in lesion detection on a uniform background with SPECT (9), and in detection of cardiac defects with SPECT (10). However, other ROC studies of lesion detection with whole-body FDG PET (11) and cardiac SPECT (12) have shown no advantage to iterative reconstruction. These conflicting results make unclear whether iterative reconstruction will be beneficial in gallium imaging, especially because human observer performance is known to be strongly task dependent (4) and none of these studies have considered lesion detection for SPECT gallium scans.

Another candidate technique for improving image quality for gallium SPECT images is patient-specific AC. Attenuation causes shadows, or regions of diminished activity, within the patient and also leads to inconsistent projection data that can increase or decrease counts in the image, especially near hot structures (13). Thus, attenuation may potentially mask a lesion or artificially enhance a noise blob, leading to both false-negative and false-positive image findings. This effect can be problematic near the hot background structures encountered in gallium imaging, especially when coupled with the large changes in tissue density found in the chest. Accurate correction for nonuniform attenuation requires estimation of patient-specific attenuation maps. Although, in the past, this estimation may have been difficult, many commercial systems are now available that can provide simultaneous or sequential transmission scans and thereby allow acquisition of coregistered attenuation maps (14). Although we know of no studies that have addressed AC in thoracic gallium imaging (1), studies of cardiac-defect detection with SPECT (10) and lesion detection with whole-body, lung, and abdominal FDG PET (15–17) have shown that correcting for the effects of attenuation may be beneficial.

Much work has been done on AC in SPECT, but the clinical usefulness of AC in gallium imaging remains an open question. Although AC may reduce the influence of attenuation artifacts, AC can also increase the magnitude and alter the texture of noise in the image, with a possible negative impact on tumor detection (18,19). Indeed, studies based on numeric measures (20,21) and human evaluation (22) have shown a mixed or no benefit to performing AC in whole-body PET. A study examining the impact of AC on the staging of malignant lymphoma using FDG PET images found no advantage to AC (23). In another study, no benefit was shown for the detection of disk objects in homogeneous backgrounds with SPECT (19). Furthermore, studies of lesion detection with whole-body FDG PET have shown decreased lesion contrast (24) and human-observer performance (11) for AC images compared with uncorrected images. With SPECT, some human-observer ROC studies have also shown a decrease in performance with corrected images (12,25).

The task in assessing gallium SPECT scans is to locate sites of gallium-avid lymphoma. Some studies have ad-

ressed similar tasks, such as tumor detection with PET or cardiac-defect detection with SPECT, but these studies were sufficiently dissimilar to the task in gallium imaging to make extension of their results difficult. The effect of attenuation compensation and iterative reconstruction on tumor detection in gallium (1) and FDG (11,16,17,20–22,24) imaging is of significant interest because of their added cost, the possible increased imaging time associated with the estimation of the attenuation maps, and the computational burden of iterative reconstruction. The purpose of this investigation was to compare FBP and OSEM, with and without AC, in gallium SPECT. The task was the detection and localization of small lesions in the chest. The diagnostic potential of the different reconstruction strategies was compared using a human-observer localization receiver operating characteristic (LROC) study.

LROC studies are an extension of the more common ROC studies that adds locating the lesion to the observer's task. The task of locating the lesion, by forcing the observer to search the image for the most probable tumor site, resembles the clinical situation with its uncertainty about tumor location. The use of a large number of tumor sites in LROC improves the generalizability of studies and limits the ability of readers to memorize the impact of attenuation artifacts on lesion appearance during training studies. An LROC study provides more information per image than an ROC study and is therefore more statistically powerful than a similar ROC study with the same number of images (26). In an LROC study, the observer does require more time to read each image than in an ROC study, but the increase in the information acquired per image is beneficial when the number of images is few or their generation is time consuming.

Our study did not exactly model the clinical situation: images were simulated assuming perfect scatter rejection, and we did not have the same degree of background variability found in a sample of actual patient images. Nevertheless, an anthropomorphic computer phantom was used with clinical noise levels, a wide variety of realistic lymphoma lesion sites throughout the thorax, and a range of lesion contrasts. As such, the format of this study provides valuable insight into the relative value of FBP, OSEM, and AC.

## MATERIALS AND METHODS

The image-generation and experimental designs of this study were similar to those of earlier studies (27,28). All images were simulated using a  $256 \times 256 \times 256$  sampling of the anthropomorphic mathematic cardiac torso (MCAT) computer phantom (29). Assignment of the background activity distribution was based on published autopsy data for the gallium distribution (30), with adjustments made, in consultation with clinicians in our department, to account for increased uptake by bone marrow. Eight sample slices through the lesion-free phantom are shown in Figure 1 along with the corresponding tissue density maps.

Projection data were generated analytically (31) and incorporated the effects of attenuation and system resolution. Separate

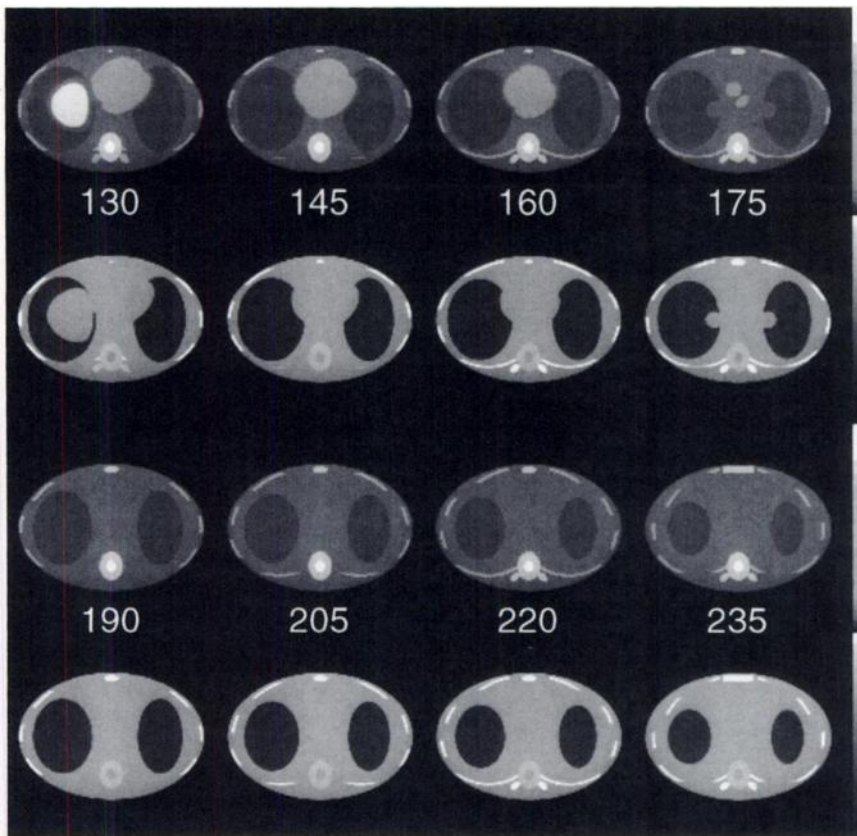


**FIGURE 1.** Eight selected transverse slices through lesion-free  $256 \times 256 \times 256$  phantom showing background activity above and corresponding attenuation map below slice index. Slices are shown in ascending order, with slice 130 being most inferior and slice 235 being most superior. These slices evenly sample portion of phantom (slices 120–240) in which lesions were placed.

projection sets were created for the 2 primary energy emissions of  $^{67}\text{Ga}$  (93 and 185 keV) using energy-specific attenuation maps. The higher energy  $\gamma$  emissions were not simulated, because they reduce image contrast (32) and are not typically acquired clinically. A single system resolution was modeled for both projection sets (33). The system resolution was experimentally measured using point sources positioned between 10 and 30 cm in front of a medium-energy general-purpose parallel-hole collimator. The point-spread functions of the point sources were fit to a 2-dimensional gaussian function whose values for full width at half maximum were linearly dependent on the distance from the collimator face. For reference, the system resolution was 10.5 mm at 10 cm. Each projection set consisted of  $128 \times 256 \times 256$  projections spanning  $360^\circ$  of rotation. The 2 projection sets were weighted by emission abundance and camera efficiency and then added together (33). The detector energy windows were assumed to be wide enough to capture all unattenuated photons. The summed projections were collapsed to  $128 \times 128$  before reconstruction. The projection data did not include the effects of scatter or septal penetration and, therefore, represent a situation of ideal scatter rejection. Although modeling of scatter is possible, we consider separate assessment of the impact of image-degrading factors, and the efficacy of their corresponding correction techniques, to be important. For this reason, scatter was not included in this study but will be incorporated into future work.

Poisson noise was added to the original noise-free projections. The mean number of photons in the projection set corresponded to the number obtained clinically in our department ( $\sim 6$  million), assuming a scatter fraction of 0.5 and perfect scatter rejection. The standard protocol of our department is to image 72 h after injection of a 10-mCi dose with a total scan time of 20 min for a  $360^\circ$

rotation. The scatter fraction was determined using a Monte Carlo simulation that included all 10 of the  $^{67}\text{Ga}$  emission photons in their appropriate abundances.

The lesions simulated in this study were all 1-cm-diameter spheres. Lesions of this size were chosen because they are the smallest that would be classified as abnormal findings on a CT scan. To introduce some variability, 3 lesion types were created, with lesion-to-soft-tissue activity ratios of 6.0:1, 8.1:1, and 10.2:1. The mid-level activity concentration was chosen, according to the results of preliminary studies, such that a median localization accuracy of 0.7 was produced (28,34). The low- and high-level activity concentrations were determined by adjusting the mid-level value by  $\pm 25\%$ . In the remainder of this article, these 3 lesion types will be referred to as low-, mid-, and high-contrast lesions. The different concentrations mimic different tumor affinities for the tracer. Because our lesion size approaches the resolution of the imaging system, small changes in size are masked by the partial-volume effect and appear in the images as changes in contrast. Thus, the 3 concentrations also mimic changes in lesion size. The low-, mid-, and high-level activity concentrations correspond to lesions with diameters of 1.1, 1.0, and 0.93 cm, respectively. Two hundred lesion sites were randomly selected from a mask of potential gallium-labeled lymphoma lesion sites that was developed in consultation with the physicians in our department. The mask included all potential lymph nodes within the chest and above the diaphragm, excluding those in the armpits because lesions there can be diagnosed without a gallium scan by palpation. The immediate vicinities of these lymph nodes were also included in the mask to allow for large tumors that have shrunk asymmetrically after treatment. One hundred of the selected sites were used to generate the 200 images (100 lesion-present images and 100

lesion-absent images) used for the LROC data acquisition. The 3 lesion types were approximately equally represented in the lesion-present images; the numbers of low-, mid-, and high-contrast lesions used were 32, 34, and 34, respectively. The remaining 100 sites were used in preliminary studies and to generate images for observer training. The large number of sites and the differences between the sites used for training and the sites used for data collection lessened the likelihood that observers would memorize site-specific attenuation artifacts and their effect on lesion appearance.

The reconstruction algorithms considered in this study were FBP and OSEM. The images reconstructed with FBP were filtered with a fifth-order 3-dimensional Butterworth filter (35) having a cutoff frequency of 0.12/pixel. Two types of AC were considered: multiplicative Chang AC, because it is a commonly used clinical correction method, and 1 iteration of iterative Chang AC (36), because it attempts to correct for inhomogeneities in the attenuation map and so might provide a fast alternative to the OSEM approaches. The images reconstructed with OSEM were filtered with a symmetric 3-dimensional gaussian function having a full width at half maximum of 3 pixels (9.5 mm). Iterative reconstruction of these images was halted after 1 iteration of OSEM using 8 subsets, corresponding to approximately 8 iterations of MLEM. The parameters of the different reconstruction strategies were optimized with respect to task performance by means of small LROC pilot studies that used the results of earlier optimization work (27,28) as a starting point. Each reconstruction strategy was applied to the same set of noisy projection data.

The attenuation map used for AC was created from the tissue density distribution in the MCAT phantom. The map was created as suggested in (33) by weighted combination of the 93- and 185-keV attenuation maps, collapsed into a  $128 \times 128 \times 128$  array. In practice, patient-specific attenuation maps would be obtained using, for example, simultaneous transmission scans and would consequently contain noise and reconstruction artifacts. The attenuation map we used represented, therefore, a best-case situation.

After reconstruction and filtering of the images, thresholds were set to improve the displayed contrast between the lesion and the background. The lower threshold was set to zero to truncate any negative values in the images. A separate upper threshold was determined for each reconstruction strategy. To calculate the upper

threshold, maximum lesion-pixel count levels were obtained for all the images processed with a particular reconstruction strategy. The SD,  $\sigma_m$ , of this set of maximums,  $S_{max}$ , was calculated, and the upper threshold was set to be the maximum of  $S_{max}$  plus  $\sigma_m$ . The setting of thresholds increased the apparent contrast of the lesion while leaving unaffected the local noise structure. This approach is similar to that in (37) except that it is based on the lesion instead of the image maximum because the object of interest in our images, the lesion, is not the hottest object in the image. Although the mean lesion-to-background contrast was 8.1:1, the partial-volume effect reduces its apparent contrast considerably because of the small size of the lesion in comparison with the spatial resolution. The threshold levels were fixed; neither they nor the monitor settings were adjustable by the observer during the study.

Examples of the images used are provided in Figures 2–4. These figures show a slice through the original phantom (the truth), with the lesion indicated by the arrow, and also the images of this slice as reconstructed using the 5 reconstruction strategies. The 3 figures show 3 lesion locations and the 3 lesion types.

Each image was reconstructed into a  $128 \times 128$  pixel array that was 1 pixel (0.317 cm) thick. The images were bilinearly interpolated to  $256 \times 256$  pixels before display and were shown on a monitor whose gray scale had been remapped to provide a log-linear relationship between luminosity and pixel value (38). The log-linear relationship was used to allow the equal discrimination of all gray levels and to increase the reproducibility of these results. The monitor was in a darkened environment sectioned off specifically for the LROC study.

Five board-certified nuclear medicine physicians were observers. For each of the reconstruction strategies, the observers were initially trained on a set of 150 images, 75 with lesions present and 75 without. For each image, the observer selected the most probable lesion site and chose a confidence rating, from a 6-category discrete scale, indicating the degree of certainty that a lesion was in the image. During training, feedback was provided in the form of a noise-free reconstruction of the image, with crosshairs indicating the true position of the lesion, if present. The study data were collected in 2 reading sessions per reconstruction strategy, each beginning with a 50-image retraining set, wherein feedback was provided, and immediately followed by a 100-image data-acquisition set with no feedback. The total time to go through

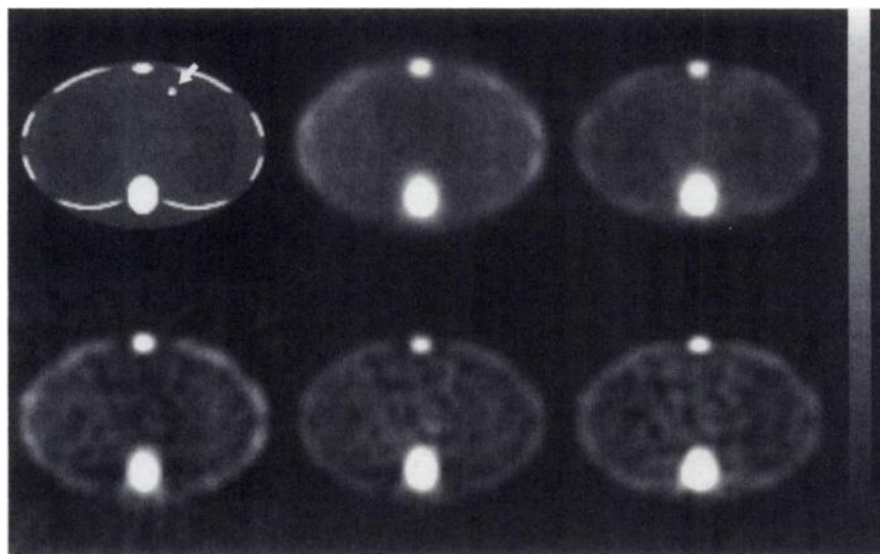


**FIGURE 2.** Example slice through original phantom (truth) and same slice reconstructed using 5 reconstruction strategies. Low-contrast lesion is indicated by arrow. From left to right and top to bottom, images shown are truth, OSEM without AC, OSEM with AC, FBP without AC, FBP with multiplicative Chang AC, and FBP with 1 iteration of iterative Chang AC.

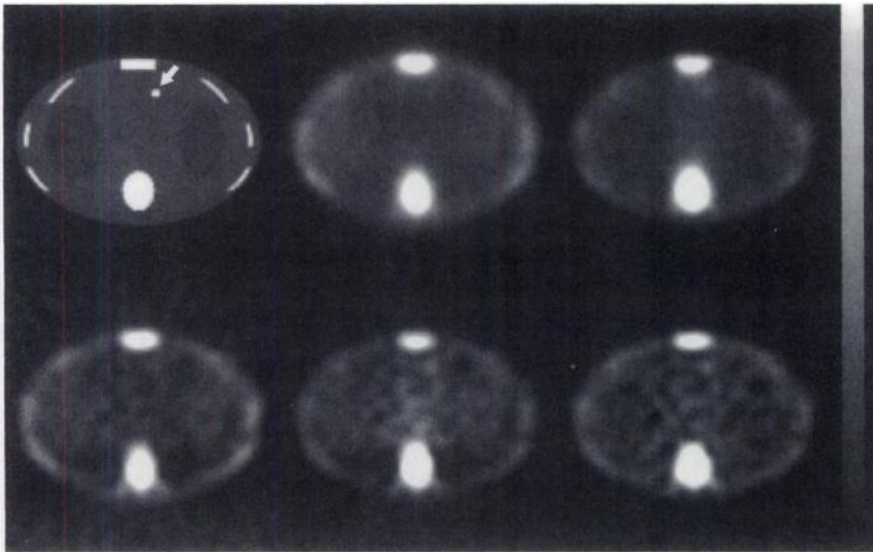


**FIGURE 3.** Example slice through original phantom (truth) and same slice reconstructed using 5 reconstruction strategies. Mid-contrast lesion is indicated by arrow. From left to right and top to bottom, images shown are truth, OSEM without AC, OSEM with AC, FBP without AC, FBP with multiplicative Chang AC, and FBP with 1 iteration of iterative Chang AC.

the 15 reading sessions (1 training and 2 study sessions for each of 5 reconstruction strategies) differed for each observer because of variations in individual availability. However, to avoid possible fatigue, observers were requested to complete no more than 2 reading sessions consecutively and to leave at least 1 h between pairs of sessions. The 3 lesion types were approximately equally represented throughout all the image sets and randomly arranged within each set. The study was designed to minimize reading order effects across observers (39).

The results of the LROC study were analyzed using the algorithm presented in (26). This algorithm uses both the localization data and the confidence ratings to simultaneously fit both LROC and ROC curves. Data for all 3 lesion types are entered into the fitting routine, and curves for the different-contrast lesions are fit concurrently. For each of the resulting fits, the algorithm then calculates the areas under the LROC ( $A_{LROC}$ ) and ROC ( $A_{ROC}$ ) curves and the probability of correct localization ( $P_{CL}$ ). The  $P_{CL}$  reflects the ability of the observer to accurately locate the center of the lesion. A small amount of observer error in indicating the lesion center is allowed and is included in the analysis through the use of a

radius of correct localization ( $R_{CL}$ ). This radius is chosen to be the breakpoint of a plot of the number of correct localizations in lesion-present images as a function of increasing the  $R_{CL}$  (28). For this study, a radius of 13 display pixels (2 cm) was used. The study data were also analyzed without regard to lesion contrast to produce a single aggregate LROC curve with corresponding  $A_{LROC}$  and  $P_{CL}$ . The  $A_{ROC}$  and  $A_{LROC}$  are related to one another by  $A_{LROC} = 2 A_{ROC} - 1$  (26), and we thus have not included the  $A_{ROC}$  data in this paper.

The LROC curves for each observer and reconstruction strategy were fit for each of the 2 viewing sets of 100 images (50 lesion-present and 50 lesion-absent images). The  $A_{LROC}$  and  $P_{CL}$  for each observer and each reconstruction strategy were subsequently averaged over the viewing sets. A 2-way ANOVA (40) was then used to search for the existence of significant differences between observers and between reconstruction strategies. Distinct ANOVAs were done for each of the 3 lesion contrasts and also for the aggregate results. The null hypothesis was that, with the same lesion contrast, the reconstruction strategies lead to equivalent mean observer performance as measured by the  $A_{LROC}$  and  $P_{CL}$ . The

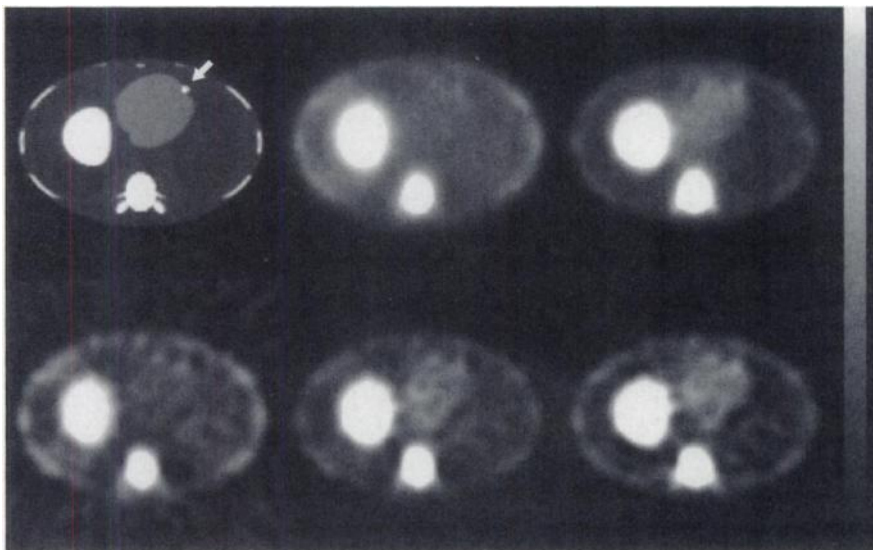


**FIGURE 4.** Example slice through original phantom (truth) and same slice reconstructed using 5 reconstruction strategies. High-contrast lesion is indicated by arrow. From left to right and top to bottom, images shown are truth, OSEM without AC, OSEM with AC, FBP without AC, FBP with multiplicative Chang AC, and FBP with 1 iteration of iterative Chang AC.

hypothesis was rejected if the probability of this occurrence was less than 5% ( $\alpha = 0.05$ ). If a significant difference existed ( $P \leq 0.05$ ), the Scheffé multiple comparisons test (40) was used to determine which pairs of reconstruction strategies were significantly different. Because the  $A_{LROC}$  and the  $P_{CL}$  were calculated independently for each reconstruction strategy, the correlation between image sets was not considered; consequently, our classification of what was significant was conservative. Although the data were analyzed with respect to  $A_{LROC}$  and  $P_{CL}$ , both metrics led to the same conclusions, so only the  $A_{LROC}$  results are presented.

## RESULTS

The LROC curves for the 3 lesion types and the 5 reconstruction strategies, averaged over observers and imaging sets, are given in Figures 5–7. In general, the curves are of similar shape and seldom cross. The curves for the high-contrast lesion (Fig. 7) do show some crossing, with curves for the 2 FBP AC reconstruction strategies behaving differently from those for the other strategies. Observer performance with the 2 FBP AC strategies is increased at low specificity but decreased at high specificity in comparison with the other reconstruction strategies.

The  $A_{LROC}$  values, averaged over observers and over the 2 image sets, are given in Table 1. Reconstruction strategies were compared for the 3 lesion contrasts and for the aggregate data. The results of these comparisons are summarized in Tables 2 and 3. These 2 tables indicate that OSEM with AC was significantly better ( $P \leq 0.003$ ), at the 2 lower lesion contrasts, than any of the other 4 techniques we tested. With the high-contrast lesion, OSEM with AC was significantly better ( $P = 0.02$ ) than FBP with multiplicative Chang AC and OSEM with no AC ( $P = 0.006$ ), but although OSEM with AC did have a higher  $A_{LROC}$  than did FBP with no AC or with iterative Chang AC, this difference was not significant ( $P > 0.05$ ).

None of the comparisons between the other 4 strategies—the 3 FBP strategies and the OSEM reconstruction without AC—resulted in significantly different ( $P < 0.05$ ) observer

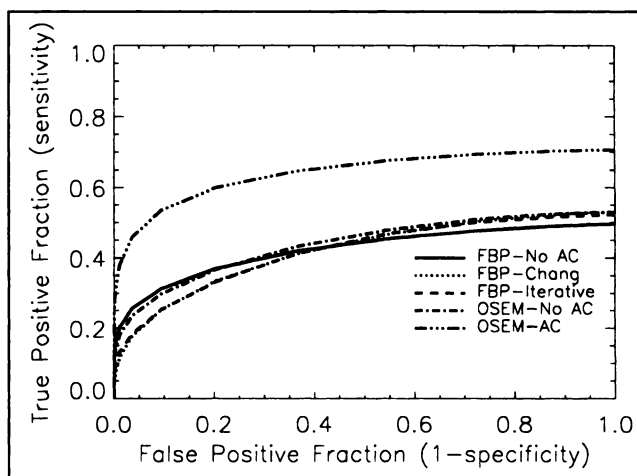


**FIGURE 6.** LROC curves for mid-contrast lesion, with 8.1:1 ratio of lesion to soft-tissue activity.

performance for any of the 3 lesion contrasts. Although differences may exist between these strategies, differences could not be distinguished with this study.

Disregarding the differences in lesion contrast reduces the number of parameters that need to be estimated to fit the LROC curve. These aggregate results might have allowed us to detect significant differences between strategies that were not visible with the lesion-specific LROC curves. However, as before, the curves show OSEM with AC as significantly better ( $P < 0.001$ ) than the 4 other techniques and no other significant differences.

## DISCUSSION

The increase in  $P$  with increased lesion contrast, for the comparisons between OSEM with AC and the other strategies, is expected and reflects the ability of all the techniques to detect lesions of adequate visibility. Consequently, OSEM with AC may not improve detection and localization in situations in which FBP is already providing accurate

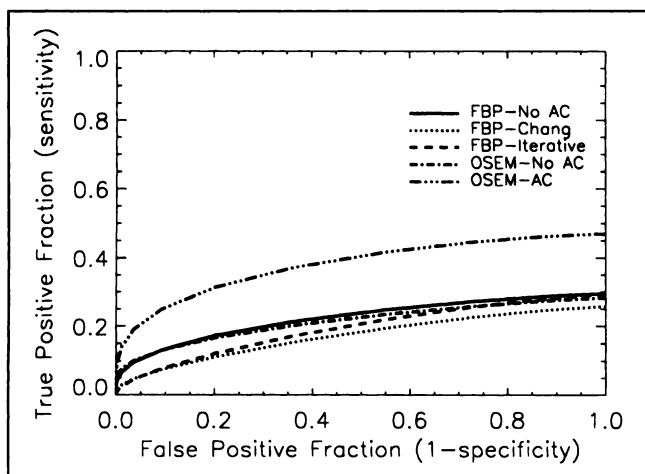


**FIGURE 5.** LROC curves for low-contrast lesion, with 6.0:1 ratio of lesion to soft-tissue activity.

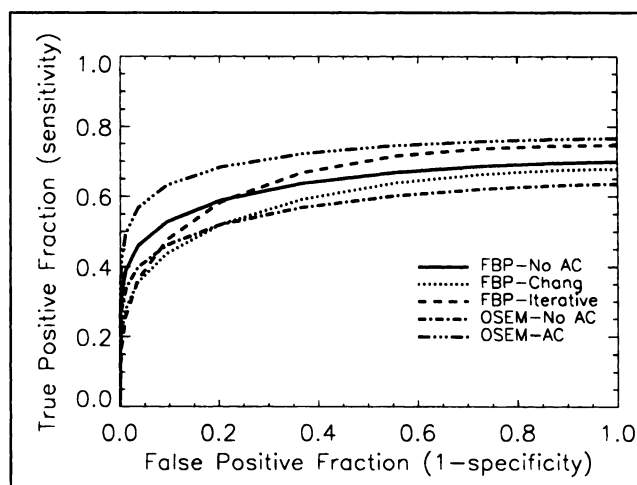


**FIGURE 7.** LROC curves for high-contrast lesion, with 10.2:1 ratio of lesion to soft-tissue activity.

**TABLE 1**  
Average  $A_{LROC}$  Values

Lesion contrast	FBP $A_{LROC}$			OSEM $A_{LROC}$	
	No AC	Multiplicative Chang AC	Iterative Chang AC	No AC	AC
6.0:1	0.22	0.17	0.19	0.21	0.38
8.1:1	0.42	0.42	0.41	0.43	0.64
10.2:1	0.63	0.59	0.65	0.57	0.71
Aggregate*	0.43	0.39	0.41	0.41	0.58

\*All data are used to fit LROC curves without regard to differences in lesion contrast.

Values are averaged over 5 observers and 2 data acquisition sets.

diagnosis. However, OSEM with AC may extend the range of detectable lesion sizes and contrasts and, consequently, provide clarity in situations in which FBP is ambiguous.

The improvement one might have expected between OSEM and FBP because of a reduction in correlation length (3) is not evident in our results. OSEM without AC is not significantly different from FBP without AC. Examining Figures 2-4, one can, however, see a change in the noise texture of the images produced by the 2 reconstruction strategies. We infer either that the correlation lengths of the OSEM and FBP reconstruction strategies were not sufficiently different or that our study was not sensitive enough to show any significant change in task performance.

We also note that AC, while improving the OSEM images significantly, did not have the same impact on the FBP images. The areas under the curve and the probability of correct localization were not significantly different among

**TABLE 2**  
Two-Way ANOVA for Average Human  $A_{LROC}$

Variation	df	m.s.	F	P
<b>Low contrast</b>				
Between strategies	4	0.0338	14.22	$4 \times 10^{-5}$
Between observers	4	0.0099	4.16	0.017
Residual	16	0.0024		
<b>Mid contrast</b>				
Between strategies	4	0.0481	18.54	$7 \times 10^{-6}$
Between observers	4	0.0551	21.24	$2 \times 10^{-6}$
Residual	16	0.0026		
<b>High contrast</b>				
Between strategies	4	0.0170	6.62	0.0024
Between observers	4	0.0548	21.37	$3 \times 10^{-6}$
Residual	16	0.0026		
<b>Aggregate*</b>				
Between strategies	4	0.0296	24.86	$1 \times 10^{-6}$
Between observers	4	0.0315	26.47	$6 \times 10^{-7}$
Residual	16	0.0012		

\*All data are used to fit LROC curves without regard to differences in lesion contrast.

df = degrees of freedom; m.s. = mean sum of squares of  $A_{LROC}$  values; F = F distribution.

**TABLE 3**  
Significance of Differences in Average  $A_{LROC}$  Between OSEM with AC and Other Reconstruction Strategies

Lesion contrast	FBP versus OSEM AC (P)			OSEM versus OSEM AC (P)
	No AC	Multiplicative Chang AC	Iterative Chang AC	No AC
Low	0.003	<0.001	<0.001	0.002
Mid	<0.001	<0.001	<0.001	<0.001
High	>0.200	0.019	>0.200	0.006
Aggregate	<0.001	<0.001	<0.001	<0.001

No significant differences ( $P \leq 0.05$ ) occurred between any FBP and OSEM reconstruction strategies without AC for any lesion contrast.

any of the 3 FBP methods tested. We interpret this finding to indicate that, for the situation modeled in this study, the increase in image noise caused by AC balanced any gains in task performance that might have resulted from a reduction in attenuation-induced artifacts. Noise is increased in the corrected images because the image areas most affected by attenuation are low-count regions with correspondingly high relative noise levels. These regions are multiplied by large Chang AC factors, leading to an increase in the absolute noise levels within the image (13). Additionally, Chang AC is only approximate (13); therefore, the benefit gained by the AC may not be as great as might have been gained with a more accurate correction method.

An important issue in assessing AC is the effect of variability in background. Changes in patient size and shape affect the location, appearance, and impact of the attenuation and reconstruction artifacts. If only a single phantom is used, with a limited number of lesion sites, it is possible for the reader to memorize the artifacts during training. Consequently, the presence of the artifacts may not degrade observer performance, and the noise added by the correction technique can lead to poorer performance. This factor may have contributed to the conflicting results obtained by different studies (10,25). A lack of background variability was a concern with our study as well. To reduce the impact, we chose multiple transverse slices from the phantom and used many different, unrepeated lesion sites. Nevertheless, all our images are of a single phantom. In future studies, we hope to further alleviate this problem using a collection of phantoms, as other investigators have done (10).

As a final caution, we reiterate that this study did not perfectly model the clinical situation: scatter was not modeled, the attenuation map contained no noise, and the use of a single computer phantom did not mirror the variability and complexity of true patient backgrounds. One should be cautious about applying these results immediately to the clinic. They are directly applicable only to the situation modeled in this study. Nevertheless, they are an

encouraging indication that OSEM with AC may improve diagnostic performance over FBP for detecting small gallium-labeled lesions in the chest. To improve on our model, we intend to incorporate scatter and consider the impact of scatter correction on this task. This study would be applicable to a situation in which scatter was rejected, so one might hypothesize that adequate scatter correction could lead to similar results. We also intend to move to hybrid-image generation, wherein computer-generated lesions are inserted into actual patient scans with normal findings.

## CONCLUSION

We investigated the impact of AC on both FBP and OSEM. Human-observer performance at detecting and localizing small gallium-labeled lesions in the chest was assessed. Three lesion contrasts were considered, and the reconstruction strategies were compared using LROC analysis.

We found no significant differences ( $P < 0.05$ ) between FBP without AC and FBP with either multiplicative Chang AC or 1 iteration of iterative Chang AC. We also found no significant differences between OSEM without AC and FBP with or without AC.

OSEM with AC was significantly better ( $P \leq 0.003$ ) than the other 4 reconstruction strategies for the 2 lower lesion contrasts considered. With the highest contrast lesion, OSEM with AC was better than the other 4 techniques but significantly better than only FBP with multiplicative Chang AC ( $P = 0.019$ ) and OSEM without AC ( $P = 0.006$ ). This improvement is thought to be caused by improvements in the modeling of the system and in the accuracy of the AC.

## ACKNOWLEDGMENTS

The authors thank Daniel deVries, Harrison H. Barrett, Arthur Burgess, Charles Metz, and Richard Swensson for helpful discussions and input. The authors also thank the reviewers for their many comments and suggestions. This study was supported by National Cancer Institute grant CA-42165. The contents are solely the responsibility of the authors and do not necessarily represent the official views of the National Cancer Institute.

## REFERENCES

- Bartold SP, Donohoe KJ, Fletcher JW, et al. Procedure guideline for gallium scintigraphy in the evaluation of malignant disease. *J Nucl Med.* 1997;38:990-994.
- van Amsterdam JAG, Kluin-Nelemans JC, van Eck-Smit BLF, Pauwels EKJ. Role of  $^{67}\text{Ga}$  scintigraphy in localization of lymphoma. *Ann Hematol.* 1996;72:202-207.
- Wilson DW, Tsui BMW. Noise properties of filtered-backprojection and ML-EM reconstructed emission tomographic images. *IEEE Trans Nucl Sci.* 1993;40:1198-1203.
- Barrett HH, Wilson DW, Tsui BMW. Noise properties of the EM algorithm: I. Theory. *Phys Med Biol.* 1994;39:833-846.
- Wilson DW, Tsui BMW, Barrett HH. Noise properties of the EM algorithm: II. Monte Carlo simulations. *Phys Med Biol.* 1994;39:847-871.
- Meikle SR, Hutton BF, Bailey DL, Hooper PK, Fulham MJ. Accelerated EM reconstruction in total-body PET: potential for improving tumour detectability. *Phys Med Biol.* 1994;39:1689-1704.
- Chan MT, Leahy RM, Mumcuoglu EU, Cherry SR, Czernin J, Chatziioannou A. Comparing lesion detection performance for PET image reconstruction algorithms: a case study. *IEEE Trans Nucl Sci.* 1997;44:1558-1563.
- Llacer J, Veklerov E, Baxter LR, et al. Results of a clinical receiver operating characteristic study comparing filtered backprojection and maximum likelihood estimator images in FDG PET studies. *J Nucl Med.* 1993;34:1198-1203.
- Tourassi GD, Floyd CE Jr, Munley MT. Improved lesion detection in SPECT using MLEM reconstruction. *IEEE Trans Nucl Sci.* 1991;38:780-783.
- LaCroix KJ, Tsui BMW, Frey EC, Jaszczak RJ. Receiver operating characteristic evaluation of iterative reconstruction with attenuation correction in  $^{99\text{m}}\text{Tc}$ -sestamibi myocardial SPECT images. *J Nucl Med.* 2000;41:502-513.
- Farquhar TH, Llacer J, Hoh CK, et al. ROC analysis of lesion detection in whole body PET: effects of acquisition mode, attenuation correction, and reconstruction algorithm [abstract]. *J Nucl Med.* 1999;40(suppl):32P.
- Gilland DR, Tsui BMW, Metz CE, Jaszczak RJ, Perry JR. An evaluation of maximum likelihood-expectation maximization reconstruction for SPECT by ROC analysis. *J Nucl Med.* 1992;33:451-457.
- King MA, Tsui BMW, Pan T-S, Glick SJ, Soares EJ. Attenuation compensation for cardiac single-photon emission computed tomographic imaging: Part 2. Attenuation compensation algorithms. *J Nucl Cardiol.* 1996;3:55-63.
- King MA, Tsui BMW, Pan T-S. Attenuation compensation for cardiac single-photon emission computed tomographic imaging: Part 1. Impact of attenuation and methods of estimating attenuation maps. *J Nucl Cardiol.* 1995;2:513-524.
- Fulham MJ, Meikle SR, Hooper PK, Silver KM. Lesion detection in whole body FDG PET using simultaneous emission transmission acquisition and OSEM reconstruction (SET-OSEM) versus emission-only (EO) and FBP reconstruction: an ROC study [abstract]. *J Nucl Med.* 1997;38(suppl):78P.
- Wahl RL, Kison P, Shreve P. Initial comparison of the accuracy of attenuation corrected vs. non-attenuation corrected FDG PET scans in evaluating the thorax of patients with suspected non-small cell lung cancer [abstract]. *J Nucl Med.* 1997;38(suppl):5P.
- Hustinx R, Dolin RJ, Benard F, et al. Impact of attenuation correction on the accuracy of FDG-PET in patients with abdominal tumors: an ROC analysis [abstract]. *J Nucl Med.* 1999;40(suppl):139P-140P.
- Moore SC, Kijewski MF, Muller SP, Holman BL. SPECT image noise power: effects of nonstationary projection noise and attenuation compensation. *J Nucl Med.* 1988;29:1704-1709.
- Soares EJ. *Attenuation, Noise, and Image Quality in Single-Photon Emission Computed Tomography* [dissertation]. Tucson, AZ: University of Arizona; 1994.
- Imran MB, Kubota K, Yamada S, et al. Lesion-to-background ratio in nonattenuation-corrected whole-body FDG PET images. *J Nucl Med.* 1998;39:1219-1223.
- Riddell C, Jousse F, Aloj L, et al. Attenuation correction vs. no attenuation correction: a signal to noise analysis in FDG PET wholebody images [abstract]. *J Nucl Med.* 1998;39(suppl):98P.
- Pieterman RM, Pruijm J, Que TH, Willemsen AT, Groen HJ, Vaalburg W. Attenuation versus non-attenuation corrected whole-body (WB) FDG-PET in the staging of non-small cell lung cancer (NSCLC) [abstract]. *J Nucl Med.* 1999;40(suppl):139P.
- Kotzerke J, Guhlmann A, Moog F, Frickhofen N, Reske SN. Role of attenuation correction for fluorine-18 fluorodeoxyglucose positron emission tomography in the primary staging of malignant lymphoma. *Eur J Nucl Med.* 1999;26:31-38.
- Bengel F, Ziegler S, Avril N, Laubenbacher C, Schwaiger M. Whole-body-PET in clinical oncology: comparison of attenuation-corrected and non-corrected images [abstract]. *J Nucl Med.* 1997;38(suppl):198P.
- Jang S, Jaszczak RJ, Tsui BMW, et al. ROC evaluation of SPECT myocardial lesion detectability with and without single iteration non-uniform Chang attenuation compensation using an anthropomorphic female phantom. *IEEE Trans Nucl Sci.* 1998;45:2080-2088.
- Swensson RG. Unified measurement of observer performance in detecting and localizing target objects on images. *Med Phys.* 1996;23:1709-1725.
- Wells RG, Simkin PH, Judy PF, King MA, Pretorius PH, Gifford HC. Effect of filtering on the detection and localization of small lesions in thoracic single photon emission computed tomography images. *Med Phys.* 1999;26:1382-1388.
- Wells RG, Simkin PH, Judy PF, et al. Maximizing the detection and localization of Ga-67 tumors in thoracic SPECT MLEM (OSEM) reconstructions. *IEEE Trans Nucl Sci.* 1999;46:1191-1198.
- Tsui BMW, Zhao XD, Gregoriou GK, et al. Quantitative cardiac SPECT reconstruction with reduced image degradation due to patient anatomy. *IEEE Trans Nucl Sci.* 1994;41:2838-2848.
- Nelson B, Hayes RL, Edwards CL, Kniseley RM, Andrews GA. Distribution of gallium in human tissues after intravenous administration. *J Nucl Med.* 1972;13:92-100.
- Pan T-S, Luo D-S, King MA. Design of an efficient 3D projector and backprojector for SPECT. In: *Proceedings of 1995 International Meeting on Fully*

- 3D Image Reconstruction in Radiology and Nuclear Medicine*. Aix-les-Bains, Savoie, France: CEA; 1994:181–185.
32. Kwan AJ, Zimmerman RE, Keech FK, O'Conner EE, Kaplan WD. Gallium-67 image contrast: relationship to energy peak and window width selection [abstract]. *Clin Nucl Med*. 1995;20:860.
  33. Pretorius PH, King MA, Pan T-S, Hutton BF. Attenuation correction strategies for multi-energy photon emitters using SPECT. *IEEE Trans Nucl Sci*. 1997;44:1323–1328.
  34. Swensson RG, Judy PF, Webster C, Seltzer SE. Nodule polarity effects on detection and localization performance in liver CT images. In: Kundel HL, ed. *Proceedings of the Society of Photo-Optical Instrumentation Engineers' International Symposium on Medical Imaging*. Vol 3036. Newport Beach, CA: SPIE; 1997:85–93.
  35. Gonzalez RC, Woods RE. *Digital Image Processing*. Reading, MA: Addison Wesley Publishing; 1992:208–209.
  36. Chang LT. A method for attenuation correction in radionuclide computed tomography. *IEEE Trans Nucl Sci*. 1978;NS-25:638–643.
  37. Tsui BMW, Terry JA, Gullberg GT. Evaluation of cardiac cone-beam single photon emission computed tomography using observer performance experiments and receiver operating characteristic analysis. *Invest Radiol*. 1993;28:1101–1112.
  38. Nawfel RD, Chan KH, Wagenaar DJ, Judy PF. Evaluation of video gray-scale display. *Med Phys*. 1992;19:561–567.
  39. Metz CE. Some practical issues of experimental design and data analysis in radiological ROC studies. *Invest Radiol*. 1989;24:234–245.
  40. Pollard JH. *A Handbook of Numerical and Statistical Techniques*. Cambridge, MA: Cambridge University Press; 1977:174–193.